Role of Molecular Architecture in Mechanical Failure of Glassy/Semicrystalline Block Copolymers: CEC vs CECEC Lamellae

T. J. Hermel,[†] S. F. Hahn,[‡] K. A. Chaffin,[§] W. W. Gerberich,[†] and F. S. Bates*[,†]

Department of Chemical Engineering and Materials Science, University of Minnesota, Minneapolis, Minnesota 55455; Dow Chemical Company, Midland, Michigan 48674; and Medtronic Corp., Brooklyn Center, Minnesota 55430

Received December 12, 2002

Revised Manuscript Received February 8, 2003

Molecular architecture affects the processing and physical properties of block copolymers in a fundamental manner. For example, ABA triblock copolymers, found in footwear, pressure-sensitive adhesives, and roofing compounds, make superior thermoplastic elastomers, while AB diblocks are virtually useless for these applications.[1−4] Multiblock $(AB)_n$ elastomeric copolymers such as poly(urethane)s provide another important example. Although the precise relationship between the number and molecular weight of hard and soft blocks, and mechanical behavior, in this category of condensation polymers is not well understood, chain architecture, i.e., $n \gg 1$, plays an important role. Microdomain alignment during flow and deformation also is influenced by block architecture, with numerous studies demonstrating qualitative differences between diblock and triblock[5−18] and recently pentablock[19,20] melts.

This communication reports our initial findings regarding the role of molecular architecture on the ultimate mechanical properties of nearly symmetric, lamellae-forming, CEC triblock and CECEC pentablock copolymers, where C and E denote poly(cyclohexylethylene) (PCHE) and poly(ethylene) (PE), respectively. Reciprocating shear was exploited to produce macroscopic sheets of aligned material with a "perpendicular" orientation.[19,20] Subsequent stress−strain measurements, directed normal to the lamellae, revealed dramatic differences in toughness that correlate with architecture. Our findings demonstrate a dramatic crossover from brittle to ductile behavior when block connectivity is increased from $n = 2$ to $n = 4$, where n signifies the number of linearly coupled diblocks.

The Dow Chemical Co. provided the CEC and CECEC copolymers used in this work. Synthesis and characterization of these saturated hydrocarbon materials are described elsewhere.[20] Greater than 99% saturation and PCHE mass fractions of 61% (CEC) and 56% (CECEC) were established using ^{1}H NMR. Monomodal and relatively narrow molecular weight distributions ($M_w/M_n \leq 1.05$) of these block copolymers were established using SEC measurements; within experimental resolution both polymers were found to be free of homopolymer and fragmented block copolymer impurities. Weight-average molecular weights of 33 800 and 51 900 g/mol for CEC and CECEC, respectively, were confirmed by light scattering. (Note the center C blocks are equal in molecular weight to the end blocks in the pentablock specimen.) Both materials exhibit glass transition and melting temperatures of $T_{g,C} \cong 145$ °C and $T_{m,E} \cong 105$ °C, respectively; DSC experiments indicated that the semicrystalline E domains contained 15−20% crystallinity. Order−disorder transition temperatures, $T_{ODT} = 231$ °C (CECEC) and $T_{ODT} = 243$ °C (CEC), were identified using low-frequency dynamic elastic modulus (G') measurements, obtained with a Rheometric ARES dynamic mechanical spectrometer.[20]

Sheets of CEC and CECEC (12 cm × 12 cm × 1.5 cm) were compression-molded at 200 °C and then aligned using a reciprocating shear device similar to that described by Koppi et al.[21] Shearing was initiated at $T_{ODT} + 7$ °C at a rate of 0.16 $s^{-1}$and a strain amplitude $\gamma = 1$. Subsequently, the specimen was cooled while shearing to $T_{ODT} - 40$ °C at 5 °C/min. After 1 h of additional isothermal shearing the device was turned off and the specimen cooled (5 °C/min) to room temperature.[22] Two-dimensional small-angle X-ray scattering (SAXS) was used to determine the melt and room temperature morphology of both materials based on established methods.[8,19,24] The shearing protocol produced a single set of "perpendicular" oriented lamellae[19,20] in all cases with layer normals coincident with the vorticity (z) axis of shear. As shown below, periodic spacings of $d \cong 18$ nm for both CEC and CECEC at 20 °C were obtained.

Tensile deformation experiments (engineering stress $\sigma = F/A_0$ vs strain $\epsilon = \Delta l/l_0$) were conducted at room temperature using a Rheometrics MINIMAT instrument operated at a crosshead speed of 10 mm/min or 0.05 s^{-1}. This communication focuses on strains applied along the lamellae normal, ϵ_z (see Figure 1a); a complete analysis of the anisotropic mechanical properties of the CEC and CECEC materials, including the strain rate dependence, will be presented in a subsequent publication. Small tensile bars with a uniform thickness of about 1.7 mm and a gauge length of 5 mm were machined from the shear-aligned sheets. This nonstandard test geometry was necessitated by the limited size of the sheets and a desire to repeat failure measurements several (five to eight) times.[25]

TEM specimens were sectioned from RuO_4 stained material taken from the gauge section of pristine and stretched samples; this staining technique was first described by Brown and Butler.[26] Two factors influence the extent of staining: permeation rate through the material and chemical reactivity. PCHE is more reactive than PE in the pristine material; hence, the glassy polymer appears darker than the semicrystalline domains in TEM images. This contrast scheme was verified using cylinder-forming CEC, which avoids the ambiguity associated with symmetric lamellae.

Figures 1 compares the tensile behavior of shear aligned CEC and CECEC, measured along the lamellae normal, i.e., σ_z vs ϵ_z. These materials are strikingly different. The triblock fails by brittle fracture at $\epsilon_{z,fail} \cong 8\%$ (Figure 1b) while the pentablock displays three distinct extension zones as labeled in Figure 1c. A recoverable elastic response at low strains (zone I, $0 \leq \epsilon_z \leq 20\%$) is followed by yielding ($\epsilon_z \cong 20\%$), then necking and drawing (zone II, $20 \leq \epsilon_z \leq 150\%$), and strain hardening (zone III, $150 \leq \epsilon_z \leq 270\%$), with rupture at $\epsilon_{z,fail} \cong 270\%$. Clearly, increasing block connectivity n, from 2 to 4, profoundly affects mechanical toughness normal to the lamellae.

Insight into the failure mechanism of the CECEC material was provided by SAXS and TEM measure-

[†] University of Minnesota.
[‡] Dow Chemical Company
[§] Medtronic Corp.

10.1021/ma021754w CCC: $25.00
Published on Web 03/11/2003

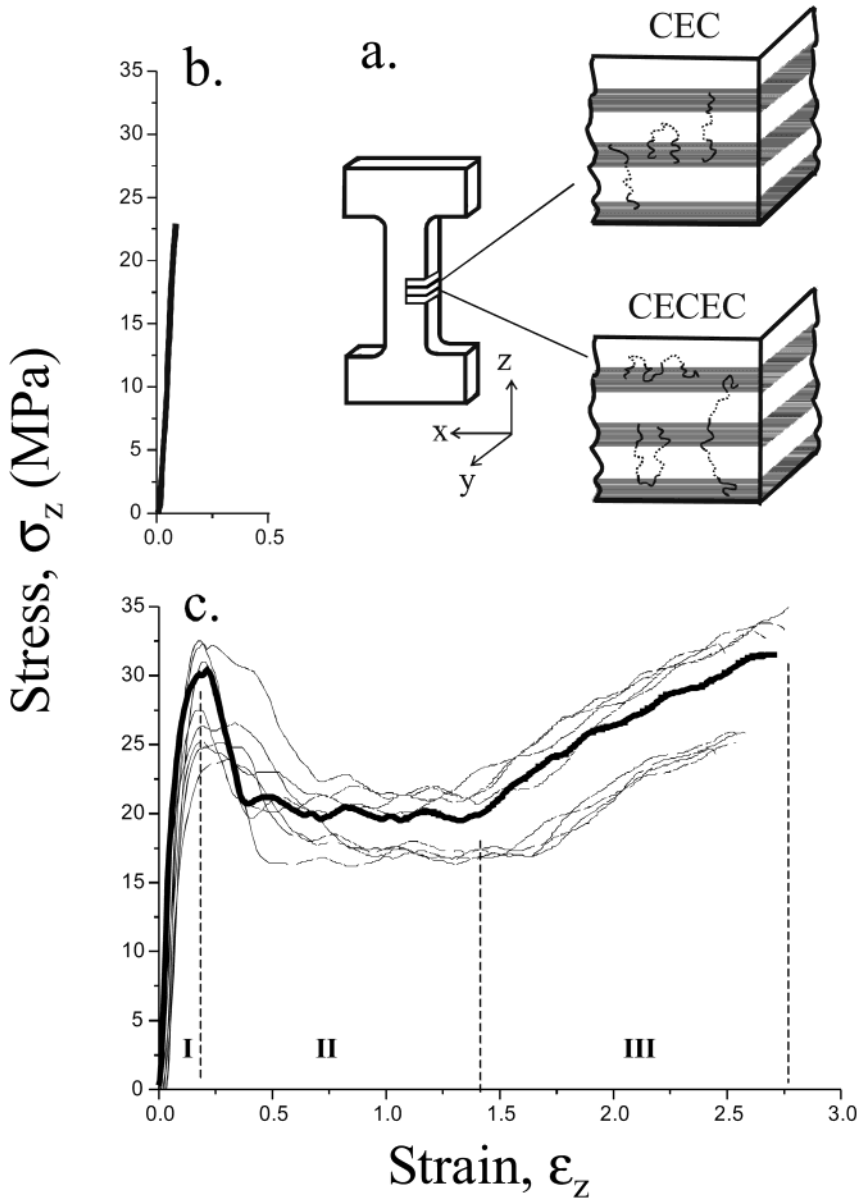

Figure 1. Tensile properties of shear aligned CEC triblock and CECEC pentablock copolymers when loaded along the lamellae normal. (a) Illustration of test geometry and representative block copolymer molecular conformations. Incorporation of a center C block in the pentablock creates bridging and entangled looping in every domain. (b) Stress−strain response for CEC. The shown response was obtained by averaging six separate measurements all of which fit within the width of the solid line. (c) Stress−strain response for CECEC. The heavy solid curve is the average of eight separate measurements represented by the lighter traces. Regions I, II, and III correspond to the elastic, necking, and strain hardening portions of the mechanical response.

ments performed before deformation, during tensile testing, and after sample failure. Figure 2 compares representative SAXS results obtained during each stage of extension with the X-ray beam directed along the *x*-axis (see Figure 1a). Prior to stretching, two diffraction spots are evident, representing the leading order reflections for the oriented lamellae, $d_0 = 2\pi/\mathbf{q_z}^* = 18.0$ nm, where $|\mathbf{q}| = q = 4\pi\lambda^{-1}\sin(\theta/2)$ is the magnitude of the scattering wavevector. (Higher order reflections were recorded when the detector was moved closer to the sample.) 17% strain results in two additional pairs of diffraction spots, which translate into 26.6 and 52.0 nm spacings. When the load in zone I was released, the initial scattering pattern and sample length were recovered; only a small fraction of the low $\mathbf{q_z}$ scattering persisted. Once the material yields, the SAXS pattern changes dramatically. In the necked region (zone II) considerable low-*q* intensity develops along with four reflections at an azimuthal angle of approximately $\phi =$ 66° relative to the stretching direction (*z*-axis) and with a *d* spacing almost indistinguishable from d_0. This pattern persists throughout necking, during strain hardening ($\phi = 68°$, $d \cong d_0$), and after failure ($\phi = 62°$, $d \cong d_0$). Little strain recovery is obtained upon unloading (or failure) after yielding.

A TEM image obtained prior to mechanical testing with the electron beam directed along the shear (*x*) direction (Figure 3a) reveals a set of uniform and well-aligned perpendicular lamellae, consistent with the SAXS pattern in Figure 2. After yielding, the TEM images are dominated by a chevron morphology, with an opening angle of about 48° (Figure 3b taken from the failed specimen). Within experimental error this corresponds exactly to the SAXS result, $\phi = (180° - 48°)/2 = 66°$. Clearly, specimen necking and drawing are accompanied by lamellae buckling. Fortuitously, certain sections of the TEM specimen absorbed excess RuO_4, producing black streaks in the micrograph. Care-

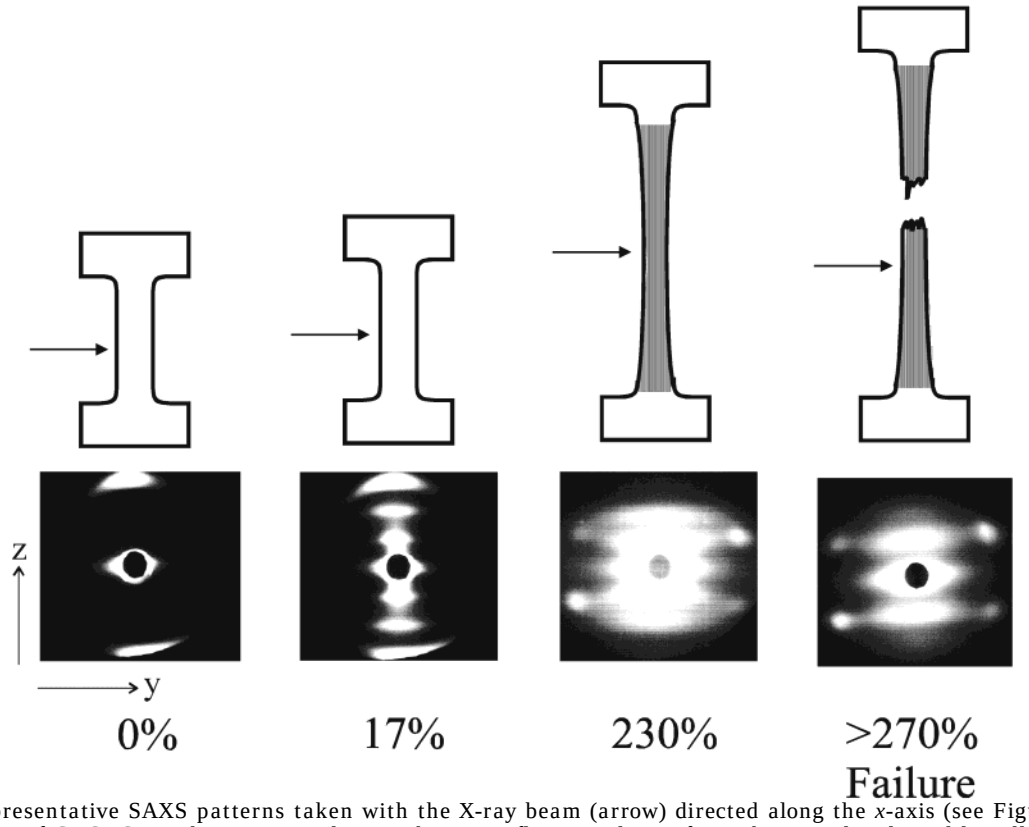

Figure 2. Representative SAXS patterns taken with the X-ray beam (arrow) directed along the *x*-axis (see Figure 1a) during tensile extension of CECEC. In the unstrained state the two reflections derive from the periodic aligned lamellae morphology with lattice spacing d_0. Application of a reversible strain (region I, Figure 1c) leads to two pairs of addition reflections consistent with a new spacing at $d = 2.9d_0$. Necking (region II) and strain hardening (region III) transforms the SAXS pattern, creating considerable low-angle scattering intensity and four new reflections at an angle $\phi \cong 66°$ relative to the *z*-axis. This irreversible transition persists through failure. Shading in the tensile bars signifies stress whitening.

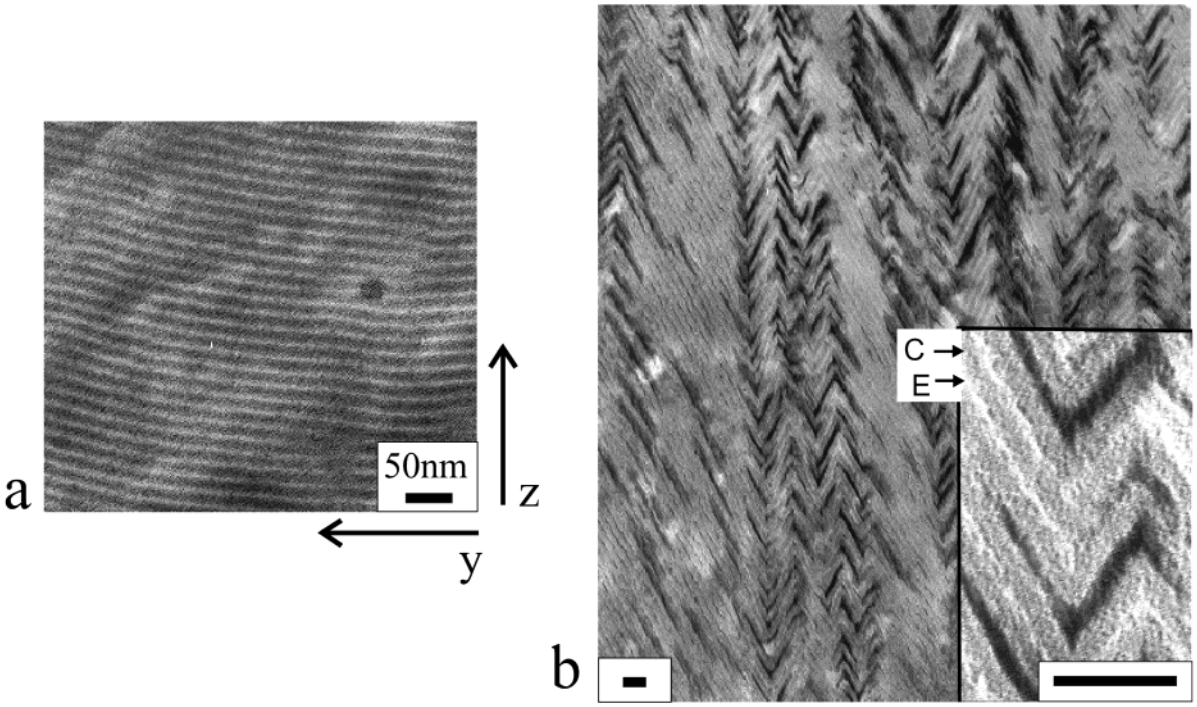

Figure 3. TEM images obtained from RuO_4 stained CECEC. Gray and white regions correspond to PCHE and PE, respectively. (a) Shear aligned but unstrained pentablock copolymer. (b) Strain hardened section of a failed CECEC specimen. The morphology is dominated by a chevron structure, with an opening angle consistent with that determined by SAXS (see Figure 2). Black streaks, highlighted in the inset image, indicate excess stain, which may result from enhanced permeability due to damage incurred during plastic deformation. This excess staining always appears in the white, hence PE, domains.

ful examination of these images reveals that this extra staining always occurs within the PE (i.e., white) domains.

On the basis of these experimental results, we propose the following failure mechanism (sketched in Figure 4) for the CECEC material. The scattering pattern at $\epsilon_z =$

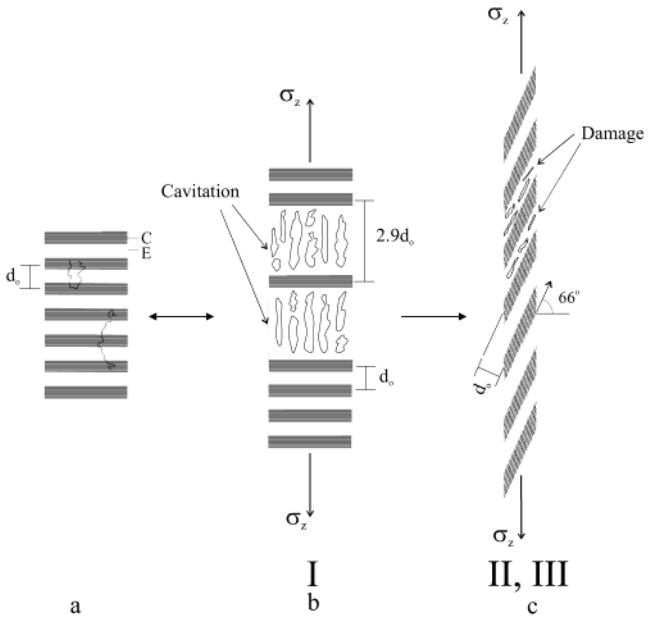

Figure 4. Proposed pentablock failure mechanism. Tensile deformation of an aligned monodomain lamellae specimen (a) results in cavitation and drawing (b) within a subset of the PE domains. Additional strain leads to a buckling instability (c) with subsequent retraction of the cavitated PE accompanied by macroscopic necking.

17% evidences two material states: pristine ($d = d_0$) and expanded ($d \cong 2.9d_0$) lamellae. Assuming no lateral contraction or PCHE expansion (i.e., incompressible glassy domains), roughly 9% of the PE domains must absorb the 17% overall strain; i.e., each deformed PE domain is extended 4.8 times. This only can be accommodated through cavitation (a familiar mode of failure in solid block copolymers[27,28]) and drawing within the PE domains. Assuming no plastic deformation of PCHE, this process should be reversible. Since all PE chains are bound to PCHE on either end, the semicrystalline domains should heal upon unloading. Increasing σ_z beyond the yield point destabilizes this partially cavitated material, leading to macroscopic buckling of the lamellae. Complete recovery of the initial PE domain thickness, $d_E \cong d_0/2$, without any material dilation, would require a maximum lamellae rotation of $\phi \cong 78°$ with an associated lateral contraction manifested as necking. The SAXS results indicate $\phi \cong 68°$.

Additional support for this mechanism is provided by Figure 3. We believe the excessively stained PE regions evidence residual damage (hence enhanced permeation of stain) that can be traced back to cavitation in the initial stages of sample deformation.

This CECEC failure mechanism contrasts sharply with that governing failure in the CEC triblock copolymer where application of stress produces brittle fracture. Presumably, failure occurs in the PCHE material which is known to be extremely brittle due to an elevated entanglement molecular weight, $M_{e,C} = 4 \times 10^3$ g/mol. Here the PCHE blocks are significantly smaller than $M_{e,C}$.

We attribute the enhanced toughness of CECEC, when strained along the lamellae normal, to the PCHE center blocks, which constitute one-third of the glassy polymer. As illustrated in Figure 1a, bridging and topologically constrained looping configurations will resist PCHE domain fracture by chain pullout. Since these center blocks are uniformly distributed throughout the material, all the lamellae will be reinforced. Just one additional covalent bond, thereby increasing n from 2 to 4, transforms the brittle triblock to a ductile pentablock material. Similar conclusions have been drawn regarding the failure of thin films of cylinder-forming CECEC triblock copolymers.[29]

Acknowledgment. This research was supported by the U.S. Department of Energy under Contract DE-AC05-960R22464.

References and Notes

(1) Argon, A. S.; Cohen, R. E.; Gebizlioglu, O. S.; Schwier, C. E. *Adv. Polym. Sci.* **1983**, *52/53*, 275−335.
(2) Allport, D. C.; Janes, W. H. *Block Copolymers*; Halsted Press: New York, 1973; p 620.
(3) Holden, G.; Bishop, E. T.; Legge, N. R. *J. Polym. Sci., Part C* **1969**, *26*, 37−57.
(4) Schweir, C. E.; Argon, A. S.; Cohen, R. E. *Polymer* **1985**, *26*, 1985−1993.
(5) Koppi, K. A.; Tirrel, M.; Bates, F. S.; Almdal, K.; Colby, R. *J. Phys. II* **1992**, *2*, 1941−1959.
(6) Koppi, K. A.; Tirrell, M.; Bates, F. S. *Phys. Rev. Lett.* **1993**, *70*, 1449−1452.
(7) Gupta, V. K.; Krishnamoorti, R.; Kornfield, J. A.; Smith, S. D. *Macromolecules* **1995**, *28*, 4464−4474.
(8) Fredrickson, G. H.; Bates, F. S. *Annu. Rev. Mater. Sci.* **1996**, *26*, 501−550.
(9) Chen, Z. R.; Kornfield, J. A.; Smith, S. D.; Grothaus, J. T.; Satkowski, M. M. *Science* **1997**, *277*, 1248−1258.
(10) Leist, H.; Maring, D.; Thurn-Albrecht, T.; Wiesner, U. *J. Chem. Phys.* **1999**, *110*, 8225−8228.
(11) Okamoto, S.; Saijo, K.; Hashimoto, T. *Macromolecules* **1994**, *27*, 5547−5555.
(12) Patel, S. S.; Larson, R. G.; Winey, K. I.; Watanabe, H. *Macromolecules* **1995**, *28*, 4313−4318.
(13) Polis, D. L.; Smith, S. D.; Terrill, N. J.; Ryan, A. J.; Morse, D. C.; Winey, K. I. *Macromolecules* **1999**, *32*, 4668−4676.
(14) Wang, H.; Newstein, M. C.; Krishnan, A.; Balsara, N. P.; Garetz, B. A.; Hammouda, B.; Krishnamoorti, R. *Macromolecules* **1999**, *32*, 3695−3711.
(15) Zhang, Y.; Wiesner, U. *J. Chem. Phys.* **1995**, *103*, 4784−4793.
(16) Winey, K. I.; Patel, S. S.; Larson, R. G.; Watanabe, H. *Macromolecules* **1993**, *26*, 2542−2549.
(17) Riise, B. L.; Fredrickson, G. H.; Larson, R. G.; Pearson, D. S. *Macromolecules* **1995**, *28*, 7653−7659.
(18) Tepe, T.; Hajduk, D. A.; Hillmyer, M. A.; Weimann, P. A.; Tirrell, M.; Bates, F. S.; Almdal, K.; Mortensen, K. *J. Rheol.* **1997**, *41*, 1147−1171.
(19) Vigild, M. E.; Chu, C.; Sugiyama, M.; Chaffin, K. A.; Bates, F. S. *Macromolecules* **2001**, *34*, 951−964.
(20) Hermel, T. J.; Wu, L.; Hahn, S. F.; Lodge, T. P.; Bates, F. S. *Macromolecules* **2002**, *35*, 4685−4689.
(21) Koppi, K. A.; Tirrell, M.; Bates, F. S.; Almdal, K.; Mortensen, K. *J. Rheol.* **1994**, *38*, 999−1027.
(22) It has been pointed in work by Roukolainen et al.[23] that cooling rate can have a dramatic effect on the mechanical response of PCHE−PE block copolymer systems. To minimize these effects, all mechanical samples presented in this work were subjected to the same cooling protocol.
(23) Ruokolainen, J.; Fredrickson, G. H.; Kramer, E. J.; Ryu, C. Y.; Hahn, S. F.; Magonov, S. N. *Macromolecules* **2002**, *35*, 9391−9402.
(24) Khandpur, A. K.; Forster, S.; Bates, F. S.; Hamley, I. W.; Ryan, A. J.; Bras, W.; Almdal, K.; Mortensen, K. *Macromolecules* **1995**, *28*, 8796−8806.
(25) Representative ASTM standard type V bars were tested and, within error, yielded stress−strain results identical to the small test specimens except for the ultimate strain to failure. Because of the higher stress concentration caused by the smaller radius of curvature between the gauge section and the grip area, the smaller test specimens tended to fail prematurely.
(26) Brown, G. M.; Butler, J. H. *Polymer* **1997**, *38*, 3937.
(27) Anderson, T. L. *Fracture Mechanics: Fundamentals and Applications*, 2nd ed.; CRC Press: New York, 1995; p 688.
(28) Askeland, D. R. *The Science and Engineering of Materials*, 3rd ed.; PWS Publishing Co.: Boston, 1994; p 812.
(29) Ryu, C. Y.; Ruokolainen, J.; Fredrickson, G. H.; Kramer, E. J.; Hahn, S. F. *Macromolecules* **2002**, *35*, 2157−2166.

MA021754W